Journal of Hazardous Materials 169 (2009) 610–620

Contents lists available at ScienceDirect

Journal of Hazardous Materials

journal homepage: www.elsevier.com/locate/jhazmat

Removal of cobalt ions from aqueous solutions by polymer assisted ultrafiltration using experimental design approach
Part 2: Optimization of hydrodynamic conditions for a crossflow ultrafiltration module with rotating part

Corneliu Cojocaru*,[1], Grażyna Zakrzewska-Trznadel, Agnieszka Miskiewicz

Department of Nuclear Methods in Process Engineering, Institute of Nuclear Chemistry and Technology, Dorodna 16, 03-195 Warsaw, Poland

ARTICLE INFO

Article history:
Received 5 November 2008
Received in revised form 14 February 2009
Accepted 31 March 2009
Available online 8 April 2009

Keywords:
Crossflow ultrafiltration
Complexation
Heavy metals removal
Response surface methodology

ABSTRACT

Application of shear-enhanced crossflow ultrafiltration for separation of cobalt ions from synthetic wastewaters by prior complexation with polyethyleneimine has been investigated via experimental design approach. The hydrodynamic conditions in the module with tubular metallic membrane have been planned according to full factorial design in order to figure out the main and interaction effects of process factors upon permeate flux and cumulative flux decline. It has been noticed that the turbulent flow induced by rotation of inner cylinder in the module conducts to growth of permeate flux, normalized flux and membrane permeability as well as to decreasing of permeate flux decline. In addition, the rotation has led to self-cleaning effect as a result of the reduction of estimated polymer layer thickness on the membrane surface. The optimal hydrodynamic conditions in the module have been figured out by response surface methodology and overlap contour plot, being as follows: $\Delta P = 70$ kPa, $Q_R = 108$ L/h and $W = 2800$ rpm. In such conditions the maximal permeate flux and the minimal flux decline has been observed.

1. Introduction

The crossflow membrane filtration processes such as microfiltration (MF) and ultrafiltration (UF) have been used in diverse industrial applications due to several distinguished advantages over conventional separation methods [1]. The membrane separation can be performed continuously under various conditions and generally requires low energy consumption. The scale-up can be executed without difficulty owing to the modular structure. Likewise, variable and easily adjusted membrane properties, as well as the possibility of hybrid processing are additional advantages. However, the concentration polarization, cake formation and membrane fouling that are intrinsic to pressure-driven membrane processes constitutes the main disadvantages of membrane filtration and cause the limitation of the use of MF and UF [1,2]. One of the effective methods to reduce these adverse phenomena is the enhancement of hydrodynamic conditions in the membrane module by promoting the turbulence close to the surface of the membrane [3]. This process known as dynamic or shear-enhanced filtration consists in creating the shear rate at the membrane surface by rotating disks [4–15], rotating membrane or filter [4,16,17], rotating shaft [3,18] or by vibration systems known also as vibratory shear-enhanced processing, VSEP [4,7,10,19–22]. Likewise, the helical, stamped or corrugated membranes as well as screw thread inserts in tubular membranes can improve the hydrodynamic conditions by producing the centrifugal instabilities called Dean vortices [2,23–26]. The most of the shear-enhanced filtration techniques have been shown to be efficient in improving MF and UF processes in terms of permeate flux increasing. The dynamic filtration systems were successfully implement in different fields of research and engineering such as chemical and environmental engineering including water, wastewater and radioactive liquid waste treatment [4,7–9,11,18–22]; biotechnological separations [4,6,10,12,13,15–17,26]; as well as medical engineering [4,27].

The polymer assisted ultrafiltration (PAUF) and micellar enhanced ultrafiltration (MEUF) can be applied successfully for wastewater treatment laden with heavy metal ions and radionuclides if it is designed properly. For instance, in the work [31] cobalt and nickel ions were simultaneously removed from aqueous feed using crossflow MEUF. Few studies [3,18] deal with the shear-enhanced PAUF process. Therefore, the further investigations on

Abbreviations: ANOVA, analysis of variances; *ARE*, average relative error; DoE, design of experiments; *EABS*, sum of the absolute errors; *ERRSQ*, sum of the square of the errors; FFD, full factorial design; *HYBRID*, hybrid fractional error function; MEUF, micellar enhanced ultrafiltration; MF, microfiltration; *MPSD*, Marquradt's percent standard deviation; PAUF, polymer assisted ultrafiltration; RSM, response surface methodology; RS-model, response surface model; UF, ultrafiltration.

* Corresponding author. Permanent address: Tudor Neculai 25, 953C-14, Iasi, Romania. Tel.: +40 742176747.
E-mail addresses: cojocaru_c@yahoo.com, ccojoc@gmail.com (C. Cojocaru).
[1] Visiting scientist under the aegis of Marie Curie Action 'Transfer of Knowledge'.

0304-3894/$ – see front matter © 2009 Elsevier B.V. All rights reserved.
doi:10.1016/j.jhazmat.2009.03.148

Nomenclature

$a_0, a_1, \ldots, a_5$	regression coefficients for polynomial equation
d	number of parameters within the regression equation
DF	degree of freedom
F-$value$	ratio of variances, computed value
i and j	subscripts (integer variables)
J	permeate flux of solution
J_A	average permeate flux
$\hat{J}_A$	predicted average permeate flux by response surface model
$J(t)_{calc}$	calculated permeate flux by means of regression equation
$J(t)_{exp}$	permeate flux, experimental value
J_W	permeate flux of pure water
K	permeability of polyelectrolyte gel layer
L_P	permeability of membrane
MS	mean square
N	the number of experimental runs for experimental design
n	number of experimental data points in flux decline curve
P_{in}	inlet (feed) side pressure
P_{out}	outlet (retentate) side pressure
P_{perm}	permeate side pressure
ΔP	transmembrane pressure
P-$value$	statistical estimator
Q_R	retentate flow rate
r	ratio of polymer (PEI) to cobalt (Co^{2+})
R^2	coefficient of multiple determination
R^2_{adj}	adjusted statistic coefficient
R_C	radius of inner cylinder
R_m	membrane resistance
R_δ	polymer layer ("cake") resistance
SS	sum of squares
S_D	cumulative flux decline
$\hat{S}_D$	predicted cumulative flux decline by response surface model
t	time
Ta	Taylor number
W	speed of rotating shaft (rotation frequency)

Greek letters

ε	annular gap
μ	dynamic viscosity of solution
ν	kinematic viscosity of solution
ω	angular speed
Ξ	valid region (region of experimentation)
ξ_1, ξ_2, ξ_3	coded levels of the factors (design variables)

this topic of research are of paramount interest to advance the state-of-art concerning the improvement of separation technologies in environmental engineering.

The most of the reported shear-enhanced filtration studies deal with the conventional methods of investigation in which one of the factors is varied maintaining the other factors fixed at constant levels. Such common methods of experimentation involve many experimental runs being time-consuming; ignore interaction effects between the considered factors and lead to low efficiency for process optimization. These restrictions of the conventional methodology of experimentation can be avoided by applying the design of experiments (DoE). The experimental design is connected to the need of minimizing the number of experiments in order to reduce the experimental cost [28]. This is very important for the experiments that include the set-up with elaborate modules or pilot scale-up. Based on the results attained according to DoE the approximation models can be developed using the response surface methodology (RSM) [29,30].

The goal of the crossflow ultrafiltration experiments using a membrane module with rotating shaft (inner cylinder) was to optimize the hydrodynamic conditions in apparatus in order to enhance the permeate flux and to reduce the fouling phenomena. In this respect, the DoE and RSM approach was used to investigate the crossflow PAUF process for cobalt–polyethyleneimine (PEI) system.

2. Materials and methods

The chemicals and analytical methods used for these investigations are the same as reported in the first part of our work. In case of crossflow PAUF experiments, a membrane module with helical Couette–Taylor flow (CTF) in the annular space between the tubular metallic membrane and the surface of rotating inner cylinder was applied to separate the cobalt ions after complexation by macromolecular ligand (PEI). Such construction of the membrane apparatus is expected to improve the hydrodynamic conditions in the module, enhance the flow and mass exchange conditions, promote turbulence as well as allow the increasing of separation efficiency and reduce the membrane fouling. In the apparatus, the SIKA-R 0.1 AS (GKN Sinter Metals) tubular metallic membrane was used with the subsequent chemical composition: 65–72% Fe, 16–18% Cr, 10–14% Ni, 2–3% Mo, and of ~0.1 μm medium pore size. The main dimensions and characteristics of the helical membrane module components were reported more detailed elsewhere [3,18].

The membrane module was a part of the experimental set-up shown in Fig. 1. The set-up was equipped with the system of rotation control in helical membrane module being composed of rotor drive with inverter Hitachi and digital display that allows the rotation frequency adjustment. The samples of the feed solution, retentate and permeate were drawn periodically from the sampling ports: F, P and R as can be seen from Fig. 1. The metallic membrane was cleaned with chemicals after each experimental run using the solutions of sodium hydroxide (NaOH, 10 g/L) and citric acid ($C_6H_8O_7{\cdot}H_2O$, 6.7 g/L). The chemical cleaning was followed by backwashing and rinsing with distilled water. The membrane cleaning procedure was repeated several times and stopped if the deviation of clean water flux was less than 5%.

3. Results and discussion

3.1. The main hydrodynamic factors for shear-enhanced ultrafiltration

The dynamic behavior of permeate flux in shear-enhanced crossflow module with rotating part (inner cylinder) is of great interest. The optimal conditions of cobalt–PEI complexation determined in the first part of the work for dead-end ultrafiltration process have been fixed for all crossflow PAUF experiments. Thus, the feed solutions with constant composition was prepared throughout all crossflow experiments, i.e. $[Co^{2+}]_0 = 65$ mg/L, $r = 5.88$ and pH 6.84. Such composition of solution, as it was shown in the first part of the work, ensures the enhanced rejection efficiency due to complexation reaction.

The hydrodynamic operational factors for shear-enhanced crossflow UF were transmembrane pressure ΔP (kPa), retentate flow rate Q_R (L/h) and the rotation frequency or speed of the rotating inner cylinder W (rpm). The operating levels of the design variables (factors) are given in Table 1. The first factor, i.e. transmembrane pressure (ΔP) is the driving force for permeate streaming in cross-

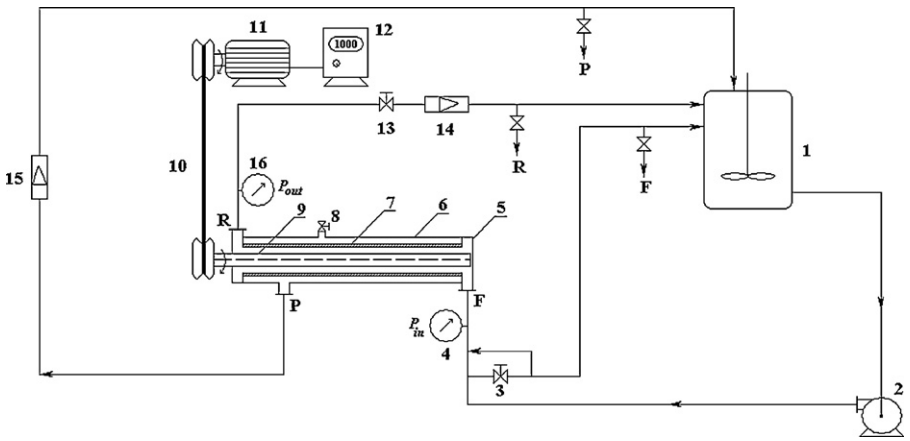

Fig. 1. Experimental set-up for crossflow PAUF 1: tank; 2: rotary pump; 3: needle valve; 4: manometer/indicator of inlet pressure P_{in} 5: membrane apparatus; 6: housing; 7: tubular membrane; 8: release vent; 9: rotor; 10: transmission belt; 11: rotor drive; 12: regulator of rotations (inverter Hitachi) with digital display; 13: needle valve; 14: flowmeter; 15: flowmeter; 16: manometer/indicator of outlet pressure P_{out}.

Table 1
Actual and coded values of design variables (factors) used for experimental design.

Design variables (factors)	Symbol of coded variable	Real values of coded levels		
		−1	0	+1
Transmembrane pressure, ΔP (kPa)	ξ_1	14	42	70
Retentate flow rate, Q_R (L/h)	ξ_2	48	78	108
Rotation frequency, W (rpm)	ξ_3	1000	1900	2800

flow ultrafiltration and is calculated as follows [32]:

$$\Delta P = \frac{P_{in} + P_{out}}{2} - P_{perm} \cong \frac{P_{in} + P_{out}}{2} \quad (1)$$

where P_{in}, P_{out}, and P_{perm} are the inlet, outlet, and permeate side pressure of membrane module, correspondingly. The second factor, retentate flow rate, gives the volume of liquid which passes through a given surface per unit time, Q_R (L/h). The last factor, i.e. the rotation speed of inner cylinder W (rpm), is responsible for enhancing of shear rate and for generation of turbulent flow. It is well known that Couette type systems, with an inner cylinder rotating inside of a concentric one, create toroidal (ring-shaped) instabilities known as Taylor vortices. The toroidal instabilities appear when the Taylor number Ta is higher than 42 and can be ascertained as [4]:

$$Ta = \frac{\omega R_C^{0.5} \varepsilon^{1.5}}{\nu} \quad (2)$$

where ω means the angular speed (s^{-1}), i.e. $\omega = 2\pi(W/60)$; R_C denotes the radius of inner cylinder (m); ε the annular gap (m) and ν is the kinematic viscosity ($m^2\ s^{-1}$). The Taylor vortices extremely enhance the mixing and when $Ta > 400$ these toroidal instabilities degenerate into turbulent flow [4]. For our specific case (i.e. $R_C = 1 \times 10^{-2}$ m, $\varepsilon = 5 \times 10^{-3}$ m and $\nu = 1.053 \times 10^{-6}\ m^2/s$) the Taylor number varied from 3516 up to 9845 according to the designed values of rotation speed W (rpm) (Table 1). Thus, the behavior of permeate flux was investigated in the turbulent flow regime created by Taylor vortices within a Couette type system.

3.2. Kinetics of permeate flux decline

The kinetics of permeate flux decline was investigated under planned hydrodynamic conditions according to full factorial design (Table 4). The obtained experimental data concerning permeate flux versus time are reported in Figs. 2–4. In addition, the regression analysis was applied to fit the experimental data by means of regression models. In our previous work [18] it was figured out that experimental kinetic data of permeate flux decline in dynamic con-

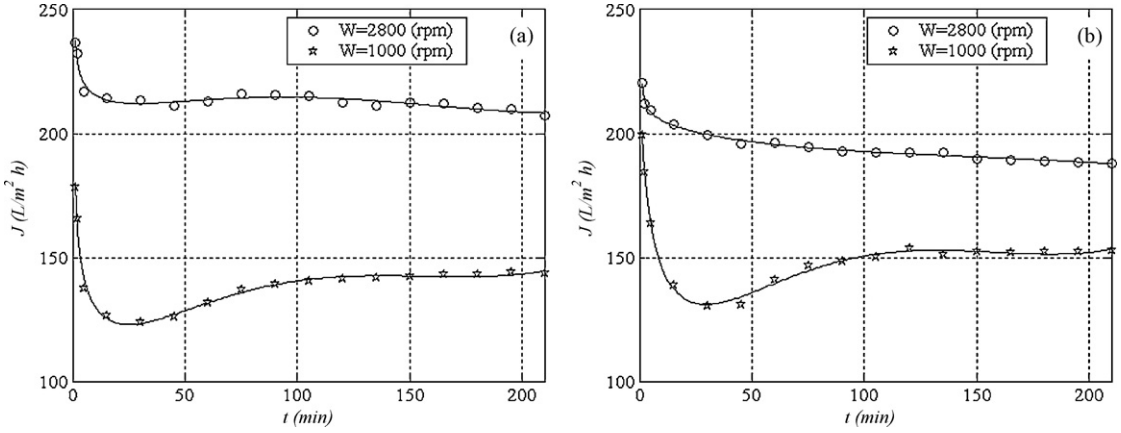

Fig. 2. Permeate flux vs. time in dynamic conditions for $\Delta P = 70$ kPa and (a) $Q_R = 108$ (L/h) and (b) $Q_R = 48$ (L/h). Solid lines: predictions given by regression models.

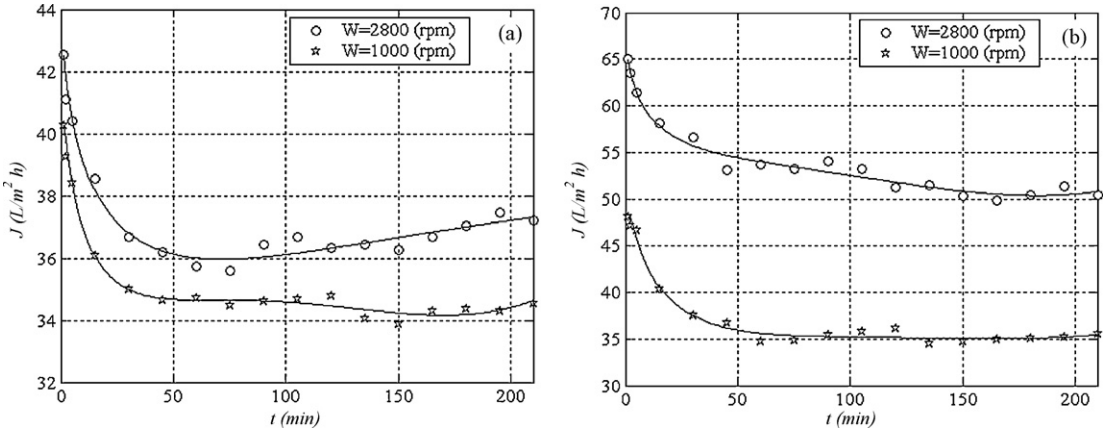

Fig. 3. Permeate flux vs. time in dynamic conditions for $\Delta P = 14$ kPa and (a) $Q_R = 108$ (L/h) and (b) $Q_R = 48$ (L/h). Solid lines: predictions given by regression models.

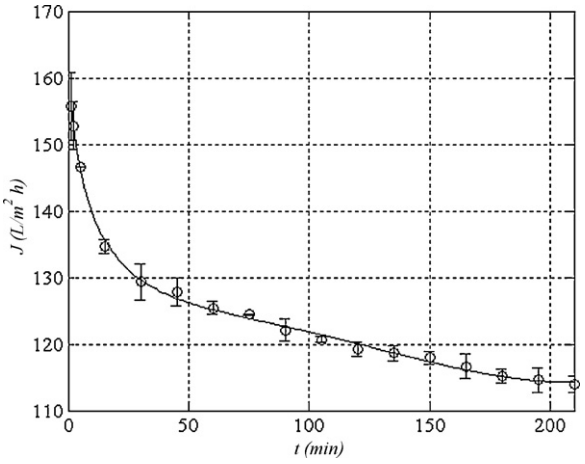

Fig. 4. Permeate flux vs. time in dynamic conditions for factors levels fixed in the center point: $Q_R = 78$ (L/h), $\Delta P = 42$ kPa and $W = 1900$ rpm. Solid line: prediction given by regression model.

ditions are fitted well by the nonlinear regression equation which can be written as

$$J(t) = a_0 + a_1\sqrt{t} + a_2 t + a_3 t^{-1} + a_4 t^2 + a_5 t^3 \quad (3)$$

The values of regression coefficients a_0, a_1, ..., a_5 for shear-enhanced crossflow PAUF experiments in case of cobalt–PEI system are reported in Table 2 and have been computed via least square method using the solver add-in with MathCAD software. The regression analysis of kinetic data was assisted by computation of different residual error functions [33] that are

- the average relative error (*ARE*):

$$ARE = \frac{100}{n}\sum_{i=1}^{n}\left(\frac{|J(t)_{exp} - J(t)_{calc}|}{J(t)_{exp}}\right)_i \quad (4)$$

- the sum of the square of the errors (*ERRSQ*):

$$ERRSQ = \sum_{i=1}^{n}(J(t)_{exp} - J(t)_{calc})_i^2 \quad (5)$$

- the hybrid fractional error function (*HYBRID*):

$$HYBRID = \frac{100}{n-d}\sum_{i=1}^{n}\left[\frac{(J(t)_{exp} - J(t)_{calc})^2}{J(t)_{exp}}\right]_i \quad (6)$$

- Marquradt's percent standard deviation (*MPSD*):

$$MPSD = 100\left[\sqrt{\frac{1}{n-d}\sum_{i=1}^{n}\left(\frac{J(t)_{exp} - J(t)_{calc}}{J(t)_{exp}}\right)_i^2}\right] \quad (7)$$

- the sum of the absolute errors (*EABS*):

$$EABS = \sum_{i=1}^{n}|J(t)_{exp} - J(t)_{calc}|_i \quad (8)$$

where $J(t)_{exp}$ denotes the experimental permeate flux; $J(t)_{calc}$ is the calculated permeate flux by means of regression equation; n is the number of data points from permeate flux decline curve (in

Table 2
Kinetic regression models developed for permeate flux predictions.

Run	Conditions	Regression models for permeate flux $J = f(t)$ and $1 \le t \le 210$ (min)
1	$\Delta P = 70$ kPa; $Q_R = 108$ L/h; $W = 2800$ rpm	$J(t) = 233.722 - 9.707\sqrt{t} + 1.172t + 12.504t^{-1} - 4.805 \times 10^{-3}t^2 + 8.744 \times 10^{-6}t^3$
2	$\Delta P = 14$ kPa; $Q_R = 108$ L/h; $W = 2800$ rpm	$J(t) = 45.203 - 2.533\sqrt{t} + 0.193t - 0.355t^{-1} - 3.437 \times 10^{-4}t^2 + 3.678 \times 10^{-7}t^3$
3	$\Delta P = 70$ kPa; $Q_R = 48$ L/h; $W = 2800$ rpm	$J(t) = 212.252 - 2.781\sqrt{t} + 0.065t + 10.277t^{-1} + 2.672 \times 10^{-4}t^{-2} - 1.051 \times 10^{-6}t^3$
4	$\Delta P = 14$ kPa; $Q_R = 48$ L/h; $W = 2800$ rpm	$J(t) = 69.824 - 4.601\sqrt{t} + 0.416t - 0.703t^{-1} - 1.648 \times 10^{-3}t^2 + 3.55 \times 10^{-6}t^3$
5	$\Delta P = 70$ kPa; $Q_R = 108$ L/h; $W = 1000$ rpm	$J(t) = 182.213 - 27.334\sqrt{t} + 3.367t + 21.291t^{-1} - 0.013t^2 + 2.386 \times 10^{-5}t^3$
6	$\Delta P = 14$ kPa; $Q_R = 108$ L/h; $W = 1000$ rpm	$J(t) = 44.759 - 3.524\sqrt{t} + 0.357t - 1.339t^{-1} - 1.318 \times 10^{-3}t^2 + 2.614 \times 10^{-6}t^3$
7	$\Delta P = 70$ kPa $Q_R = 48$ L/h $W = 1000$ rpm	$J(t) = 238.02 - 44.797\sqrt{t} + 5.143t + 0.759t^{-1} - 0.019t^2 + 3.357 \times 10^{-5}t^3$
8	$\Delta P = 14$ kPa; $Q_R = 48$ L/h; $W = 1000$ rpm	$J(t) = 59.287 - 6.901\sqrt{t} + 0.586t - 5.213t^{-1} - 1.628 \times 10^{-3}t^2 + 2.698 \times 10^{-6}t^3$
9 and 10	$\Delta P = 42$ kPa; $Q_R = 78$ L/h; $W = 1900$ rpm	$J(t) = 170.352 - 13.21\sqrt{t} + 1.173t - 2.563t^{-1} - 4.164 \times 10^{-3}t^2 + 7.841 \times 10^{-6}t^3$

Table 3
The error functions employed in regression analysis.

Run	*ARE*	*ERRSQ*	*HYBRID*	*MPSD*	*EABS*
1	0.626	45.84	1.899	0.931	23.109
2	0.538	1.114	0.275	0.866	3.380
3	0.325	10.832	0.491	0.496	10.983
4	1.016	7.913	1.354	1.598	9.191
5	0.865	51.626	3.164	1.467	21.273
6	0.322	0.432	0.114	0.578	1.888
7	0.673	27.998	1.799	1.131	16.738
8	1.132	5.180	1.208	1.776	7.392
9 and 10	0.348	4.887	0.352	0.529	7.421

our case $n = 17$) and d the number of parameters within the regression equation (i.e. $d = 6$). The computed values of error functions are reported in Table 3. As one can see, the experimental data are fitted well by regression equations with a fitting error lower than 1.132% in terms of *ARE* and lower than 1.776% in terms of *MPSD*.

The results from Figs. 2–4 show the dependence of permeate flux versus time for different hydrodynamic conditions where the special emphases are put on the influence of rotation frequency. Thus, the increasing of rotation speed leads obviously to higher permeate fluxes and lower flux decline. This fact can be attributed to minimization of both concentration polarization and fouling phenomena with the increment of rotation speed as a result of enhancement of hydrodynamic conditions and promotion of turbulence near to the surface of tubular membrane. As expected, the growth of transmembrane pressure from 14 to 70 kPa also conducts to improvement of permeate flux. The data from Fig. 2 reveal that for the conditions of $\Delta P = 70$ kPa and $W = 2800$ rpm, permeate fluxes are the highest and the flux decline is the most reduced because of high turbulence flow in apparatus. For a lower rotation speed of $W = 1000$ rpm, a marked flux decline can be seen at the first moments ($t < 30$ min). After that, i.e. for $t > 30$ min, permeate flux starts to increase as a result of self-cleaning effect of membrane surface that appears with time. The improvement of permeate flux due to self-cleaning effect is valid for the time interval of $30 \leq t \leq 120$ min. After this time period, permeate flux has a trend of stabilizing (steady state). Thus, the shear-enhanced ultrafiltration process that involve the self-cleaning effect can be segmented in three distinguished parts over the time interval according to achieved experimental data for $\Delta P = 70$ kPa and $W = 1000$ rpm (Fig. 2). In the first stage, related to initial moments $t < 30$ min, the permeate flux drop is noticeable because of the transmembrane pressure effect. For the second stage, i.e. $30 \leq t \leq 120$ min, permeate flux begins to rise as a result of stronger effect of rotation frequency that is developed within time. The last stage, given by $t > 120$ min, is characterized by stabilizing of permeate flux as a result of achieving of equilibrium state between the effects of transmembrane pressure and rotation speed. Fig. 3 reports permeate fluxes versus time for a transmembrane pressure of 14 kPa. In this case the self-cleaning effect is not as obvious as for $\Delta P = 70$ kPa and permeate flow seems to be more unstructured because of low transmembrane pressure. Fig. 4 illustrates the kinetics of permeate flux when design variables were hold at their central levels. In such conditions the replication of experiments was performed to determine the average values of permeate flux in each point as well as the corresponding errors bars. The replication error is higher in the first moments.

In addition, the normalized permeate flux (or relative flux) was determined as the ratio between permeate flux of solution J (L/m^2 h) and that of pure water J_W (L/m^2 h) recorded in the same hydrodynamic conditions. Likewise, the permeability of membrane L_P (L/m^2 h kPa) for different hydrodynamic conditions was calculated as permeate flux J (L/m^2 h) divided by the transmembrane pressure ΔP (kPa). The normalized fluxes as well as membrane permeabilities are reported in Fig. 5 for a transmembrane pressure of 70 kPa and for different shear-enhanced conditions. The results shown in Fig. 5 indicate that the increasing of rotation frequency in the module leads to the improving of both permeate normalized flux and membrane permeability.

3.3. Approximation of gel layer formation

According to resistance-in-series model, permeate flux depends on the cake layer and membrane resistance. In case of PAUF experiments, the cake layer is equivalent with polymer layer formation. Thus, permeate flux can be expressed as a function of total membrane-polymer ("cake") resistance by using the following equation [3]:

$$J(t) = \frac{\Delta P}{\mu[R_m + R_\delta(t)]} \tag{9}$$

where R_m and R_δ denotes the membrane resistance and polymer layer ("cake") resistance, respectively; μ is the dynamic viscosity of the liquid (solution). In our case the viscosity of solution was

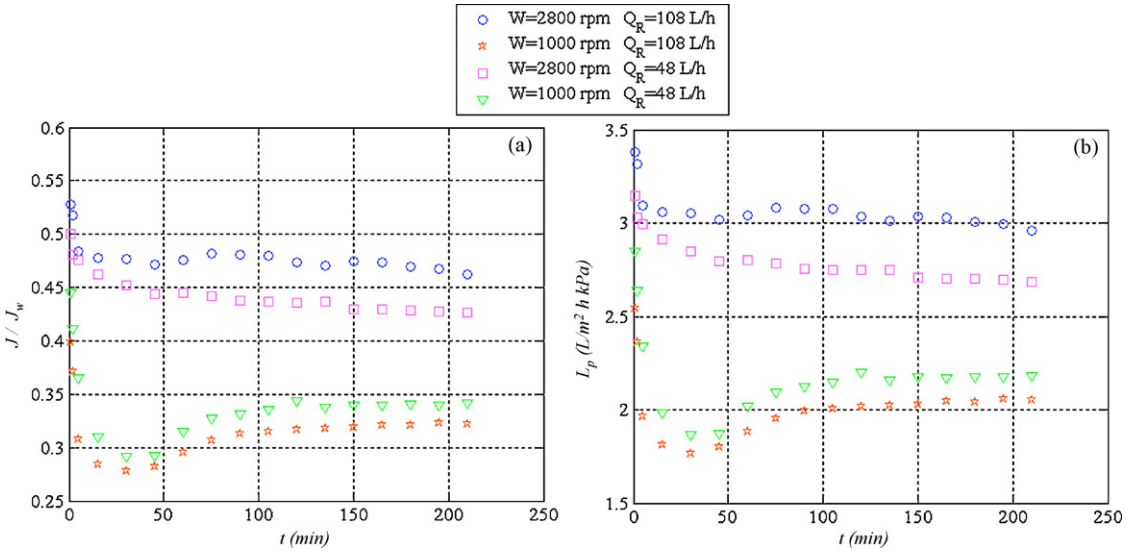

Fig. 5. Normalized permeate flux (a) and membrane permeability (b) vs. time for $\Delta P = 70$ kPa and different hydrodynamic conditions in the membrane module.

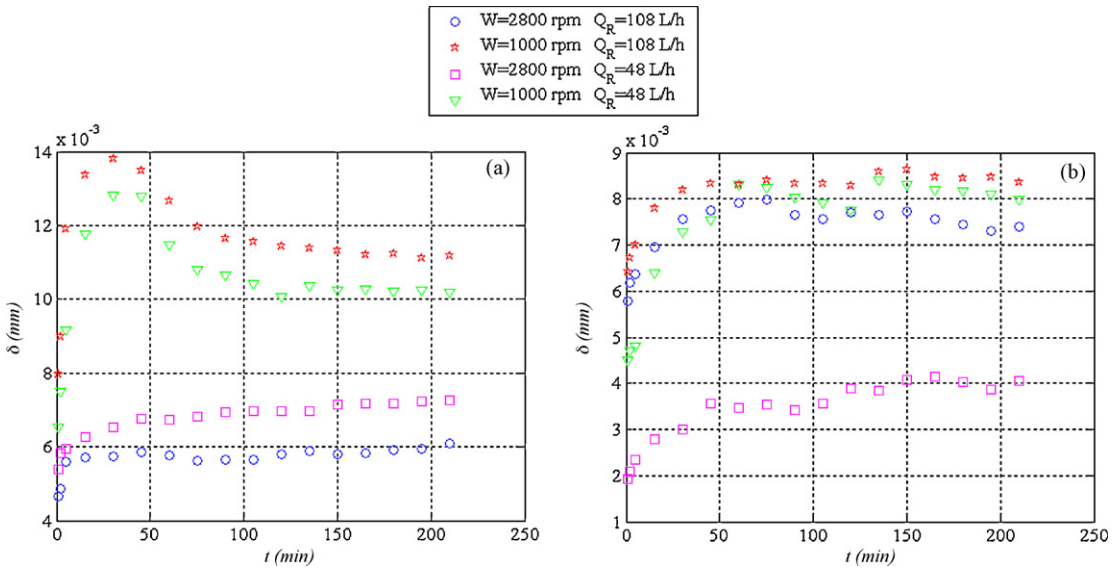

Fig. 6. Appraisal of boundary layer thickness developed in time for different experimental conditions: (a) $\Delta P = 70$ kPa and (b) $\Delta P = 14$ kPa.

determined experimentally at temperature of $25 \pm 1\,^{\circ}C$ by using a Ubbelohde viscometer and it was equal $\mu = 1.05 \times 10^{-3}$ Pa s. The membrane resistance was estimated from water permeability and was found to be $R_m = 5.4 \times 10^{11}\ m^{-1}$. The polymer layer resistance R_δ was determined from Eq. (9) as follows:

$$R_\delta(t) = \frac{\Delta P}{J(t)\ \mu} - R_m \tag{10}$$

The thickness of the residual deposit layer was estimated by the subsequent equation:

$$\delta(t) = K\, R_\delta(t) \tag{11}$$

where K-value for the polymer layer was assumed as $K = 10^{-17}\ m^2$ and represents the permeability of polyelectrolyte gel layer according to Ref. [3]. The approximation of K-value was considered just to ascertain the influence of the rotation on permeate flux and to reveal the tendency of δ-value variation. The thickness of the deposit layer formed by the polymer medium on the membrane surface determined for different operating conditions and with assumption that $K = 10^{-17}\ m^2$, was in the range of 1.9–14 μm for dynamic conditions in apparatus. The variation of polymer layer thickness showed the evident influence of rotation: the δ-values decreased with increment of rotation frequency in the helical-flow membrane apparatus (Fig. 6). This fact is the evidence that by promoting the turbulence in apparatus, the resistance of boundary layer and the resistance of the deposit accumulated on the membrane surface are reducing. Also, the self-cleaning effect is observed in terms of δ-value variation. The polymer layer formed in first moments is followed by the decreasing of its thickness (Fig. 6). Even if one considered the estimated values of the thickness δ only as approximated ones, the influence of the rotation motion was obvious.

3.4. Experimental design and response surface modeling

In order to investigate the main and interaction effects of the hydrodynamic factors upon the performance of shear-enhanced crossflow ultrafiltration process two responses have been derived from experimental curves of permeate flux decline. The first considered response was the average permeate flux J_A that have been calculated by integration of $J(t)$ regression function from $t_1 = 1$ min up to $t_n = 210$ min as follows:

$$J_A = \frac{1}{t_n} \int_{t_1}^{t_n} J(t)\, dt \tag{12}$$

where the regression functions $J(t)$ of permeate flux given by regression analysis are reported in detail in Table 2 for different hydrodynamic conditions planned according to factorial design.

The second response was chosen to quantify the intensity of fouling phenomena in dynamic conditions given by rotating inner cylinder in the membrane module. In this respect, the cumulative flux decline (S_D) was considered as the most suitable response in this case, being defined in our previous work as [18]:

$$S_D = \sum_{j=2}^{n} \left(\frac{J_1 - J_j}{J_1} \right) \tag{13}$$

where J_1 denotes the permeate flux measured in the first moment ($t_1 = 1$ min) and J_j is the permeate flux measured in the next moments $t_j > t_1$. The S_D-response gives information about the evolution of permeate flux from initial to final moment of the experiment. Therefore, this response is suitable for the estimation of fouling phenomena in the dynamic conditions (membrane modules with rotating part) when turbulence flow pattern may lead to self-cleaning effect of the membrane surface and the evolution of flux is very important. The design of experiments used for statistical modeling of PAUF process is reported in Table 4, which includes $N = 10$ experimental runs.

Based on factorial design (Table 4) the interaction response models in terms of coded variables were constructed by means of multiple linear regression method [29,30]. After testing the significance of all regression coefficients by Student's t-test the response surface models (RS-models) in terms of coded variables are as follows:

$$J_A = 106.023 + 66.033\xi_1 - 1.063\xi_2 + 17.515\xi_3 + 3.343\xi_1\xi_2 + 12.835\xi_1\xi_3 + 1.735\xi_2\xi_3 + 5.41\xi_1\xi_2\xi_3 \tag{14}$$

$$\hat{S}_D = 2.652 - 0.382\xi_2 - 0.622\xi_3 + 0.195\xi_1\xi_2 - 0.403\xi_1\xi_3 \quad \text{subjected to: } \xi_i \in \Xi;\quad \Xi = \left\{ \xi_i \,\middle|\, -1 \le \xi_i \le +1 \right\};\quad \forall i = \overline{1,3} \tag{15}$$

Table 4
Full factorial design (FFD) for crossflow PAUF process.

Run number (N) and type[a]		Factors (controllable input variables)						Responses	
		Transmembrane pressure		Retentate flow rate		Rotation frequency		Average permeate flux	Cumulative flux decline
		ΔP (kPa)	Level[b] ξ_1	Q_R (L/h)	ξ_2	W (rpm)	ξ_3	J_A (L/m^2 h)	S_D
1	O1	70	1	108	1	2800	1	211.83	1.530
2	O2	14	−1	108	1	2800	1	36.59	2.020
3	O3	70	1	48	−1	2800	1	192.98	1.818
4	O4	14	−1	48	−1	2800	1	52.75	2.751
5	O5	70	1	108	1	1000	−1	136.84	3.494
6	O6	14	−1	108	1	1000	−1	34.58	2.036
7	O7	70	1	48	−1	1000	−1	146.57	3.956
8	O8	14	−1	48	−1	1000	−1	36.04	3.611
9	C1	42	0	78	0	1900	0	122.01	2.865
10	C2	42	0	78	0	1900	0	122.31	2.988

[a] O = orthogonal design points, C = center points.
[b] −1 = low value, 0 = center value, +1 = high value.

Table 5
Analysis of variance (ANOVA) for response surface model (response: J_A, average flux).

Source	DF[a]	SS[b]	MS[c]	F-value	P-value	R^2	R^2_{adj}
Model	7	38906.74	5558.105	21.334	0.0455	0.987	0.941
Residual	2	521.04	260.522				
Total	15	39427.78					

[a] Degree of freedom.
[b] Sum of squares.
[c] Mean square.

Table 6
Analysis of variance (ANOVA) for RS-model (response: S_D, cumulative flux decline).

Source	DF	SS	MS	F-value	P-value	R^2	R^2_{adj}
Model	4	5.968	1.492	32.095	0.0009	0.963	0.933
Residual	5	0.232	0.046				
Total	9	6.20					

where ξ_i denotes the coded variable and Ξ means the valid region also known as region of experimentation. In terms of actual variables the RS-models are written as follows:

$$\hat{J}_A = -8.58 + 2.14\Delta P + 0.25Q_R + 0.017W - 9.6\times10^{-3}\Delta PQ_R - 4.9\times10^{-5}\Delta PW - 2.4\times10^{-4}Q_RW + 7.2\times10^{-6}\Delta PQ_RW \quad (16)$$

cumulative flux decline (S_D) in the studied region of experimentation of operating variables (transmembrane pressure, retentate flow rate and rotating frequency of the rotor). The experimental data plotted against the predicted ones for both interaction models are illustrated in Fig. 7. The goodness-of-fit between experimental and predicted data is evident. Likewise the average relative error in percentage was calculated for both models. The average relative errors of 2.64% and 6.19% were achieved in case of average permeate flux and cumulative flux decline, respectively. The obtained average relative errors were lower than 7% for both regression models considered.

$$\hat{S}_D = 4.44 + 1.23\times10^{-2}\Delta P - 2.25\times10^{-2}Q_R - 1.91\times10^{-5}W + 2.32\times10^{-4}\Delta PQ_R - 1.60\times10^{-5}\Delta PW$$
$$\text{subjected to}: \quad 14 \le \Delta P \le 70 \text{ kPa}; \quad 48 \le Q_R \le 108 \text{ L/h}; \quad 1000 \le W \le 2800 \text{ rpm} \quad (17)$$

In order to check the statistical significance of interaction RS-models the analysis of variance (ANOVA) was employed (Tables 5 and 6).

According to ANOVA tables both models are statistically significant and can be used for the prediction of average flux (J_A) and

The response surface plots and contour line maps for both response functions, i.e. $\hat{J}_A$ and $\hat{S}_D$ are presented in the next figures (Figs. 8–13). The graphical response surface analysis resulted from Figs. 8–10 indicates that increasing of both transmembrane

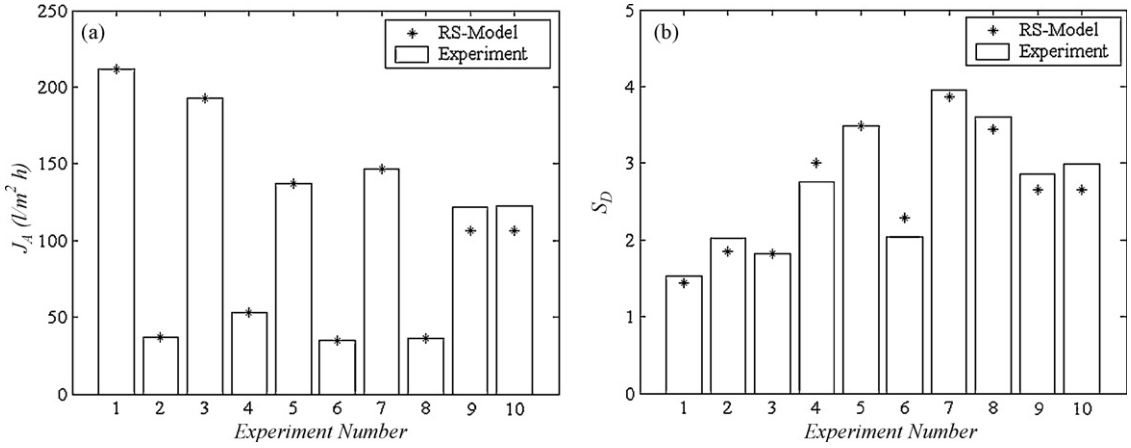

Fig. 7. Experimental data plotted against the predicted ones for both responses (a) average permeate flux and (b) cumulative flux decline.

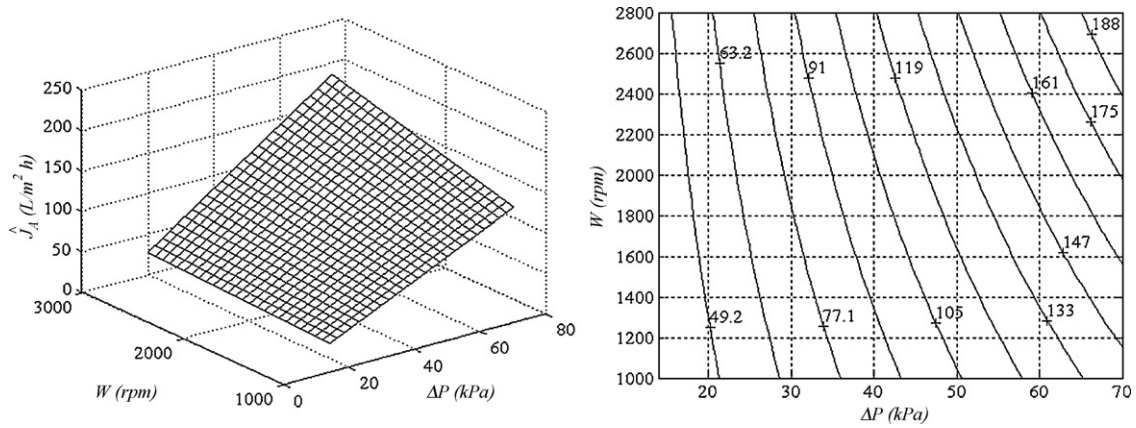

Fig. 8. $\hat{J}_A$-response surface plot and contour-line map depending on W and ΔP variables, holding the other variable at its center level Q_R = 78 L/h.

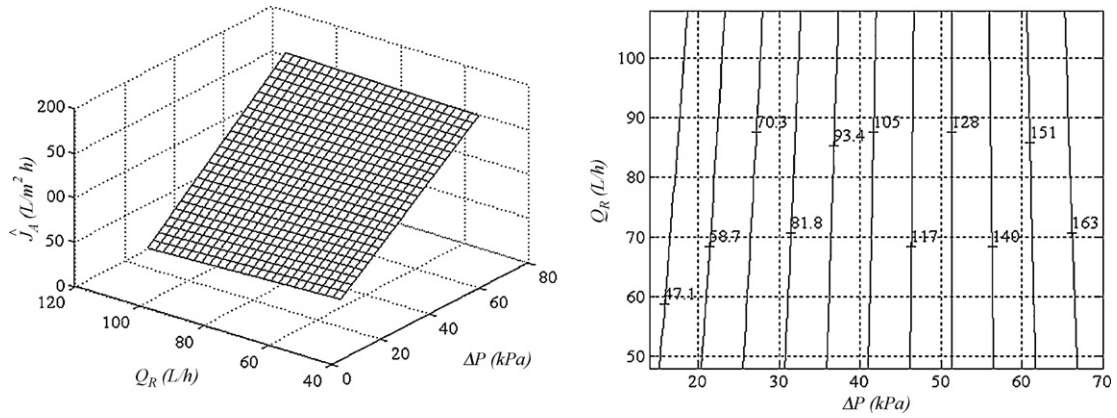

Fig. 9. $\hat{J}_A$-response surface and contour-line plots depending on ΔP and Q_R variables, holding the other variable at its center level W = 1900 rpm.

pressure ΔP (kPa) and rotating frequency W (rpm) conducts to enhancing of permeate flux (average value). The third factor (retentate flow rate Q_R) has the utmost reduced influence upon average flux in dynamic conditions than the other two factors. Also, the interaction effects between this factor and the other two are more significant than the main effect of Q_R. According to response surface plots, the increment of retentate flow rate in the dynamic conditions leads mainly to decreasing of permeate flux especially for lower operating pressure (ΔP < 50 kPa) and for lower rotating frequency. Similar observation, related to increasing of permeate flux with decreasing of retentate flow rate in dynamic conditions, was noted in our previous work [18] dealing with copper removal by PAUF in helical module using polyacrilic acid as chelating agent. In this case (cobalt–PEI system) at higher transmembrane pressure and intensive rotations the slight increasing of permeate flux with increment of retentate flow rate was also noted. It is worthy to note that the influence of retentate flow rate on permeate flux in the dynamic conditions (membrane module with rotating parts) is different than the influence in conventional systems (without rotating parts) and the further investigations should be carried out to understand better its complexity. According to response surface plot depicted in Fig. 8 the strong interaction effect occurs between applied pressure ΔP and rotating frequency W, i.e. the increasing of transmembrane pressure it is more significant at higher rotation

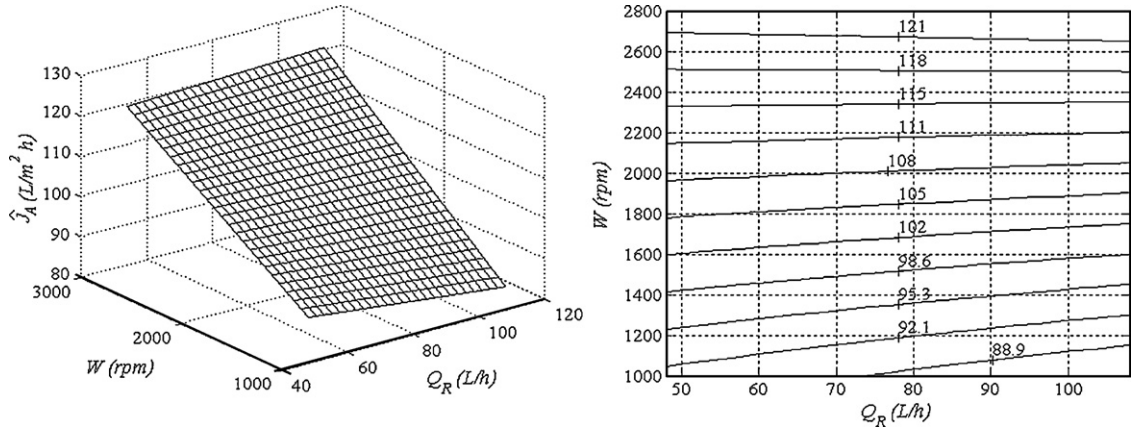

Fig. 10. $\hat{J}_A$-response surface and contour-line plots depending on W and Q_R variables, holding the other variable at its center level ΔP = 42 kPa.

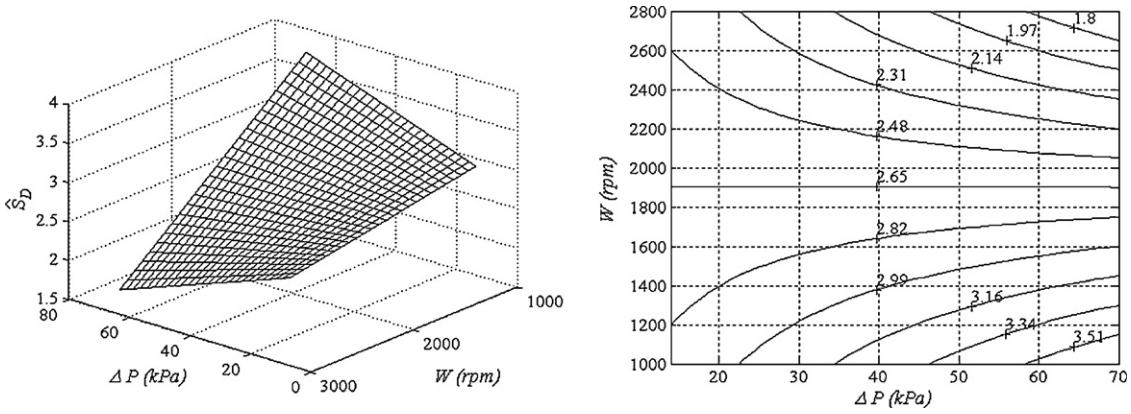

Fig. 11. $\hat{S}_D$-response surface and contour-line plots depending on W and ΔP variables, holding the other variable at its center level Q_R = 78 L/h.

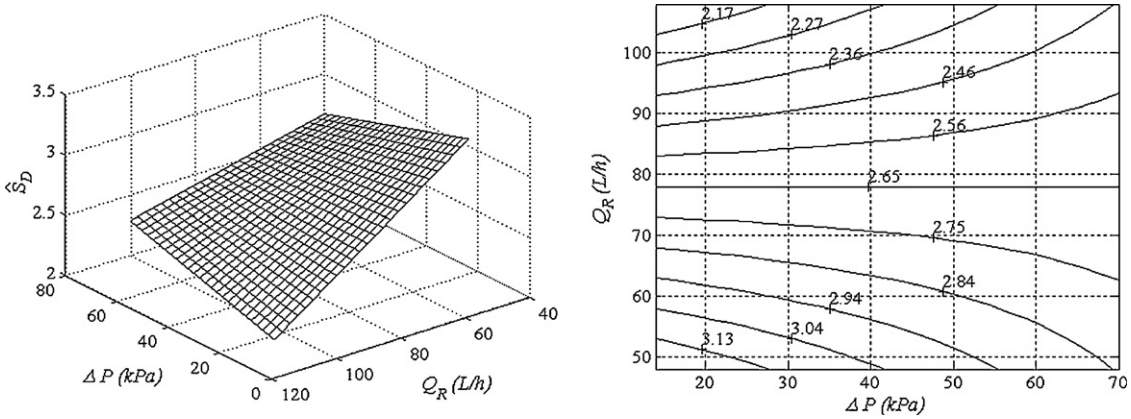

Fig. 12. $\hat{S}_D$-response surface and contour-line plots depending on ΔP and Q_R variables, holding the other variable at its center level W = 1900 rpm.

frequency as well as the influence of rotation is more important at higher applied pressure. These interaction effects between ΔP and W conduct to enhancing of permeate flux.

In Figs. 11–13, the response surface plots and contour maps for cumulative flux decline are presented. The most important effect in this case is attributed to the speed of rotating shaft that obviously reduces the fouling phenomena. Thus, the increasing of rotating frequency W gives lower values of the cumulative flux decline. The main effect of transmembrane pressure upon S_D-response is not significant in dynamic conditions for this system (Co–PEI), at least for the investigated region of 14–70 kPa. In spite of this, the applied pressure plays an essential role in the interaction effects together with other factors, i.e. rotation frequency and retentate flow rate. For example, at lower rotation frequency (W < 1900 rpm) the increasing of applied pressure leads to increasing of cumulative flux decline (the fouling phenomena are favored). At very high rotation frequency (W > 2500 rpm) the main effect of W factor is too strong and the increasing of transmembrane pressure conducts to decreasing of cumulative flux decline S_D.

Since the highest rotation frequency conducts to improving of permeate flux as well as leads to minimization of the cumulative flux decline the overlap contour plot were drawn for both responses J_A and S_D at the rotation level of W = 2800 rpm (Fig. 14). This plot was carried out in order to identify the optimal region.

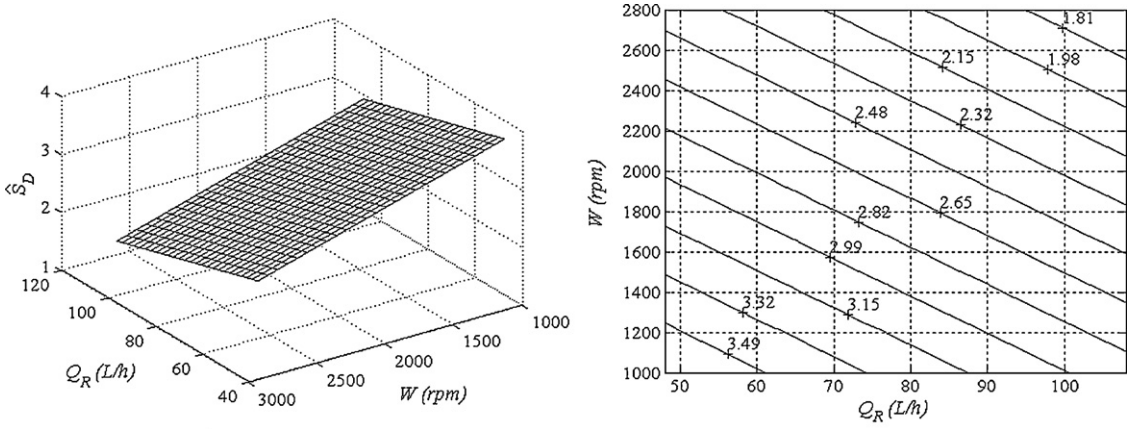

Fig. 13. $\hat{S}_D$-response surface and contour-line plots depending on W and Q_R variables, holding the other variable at its center level ΔP = 42 kPa.

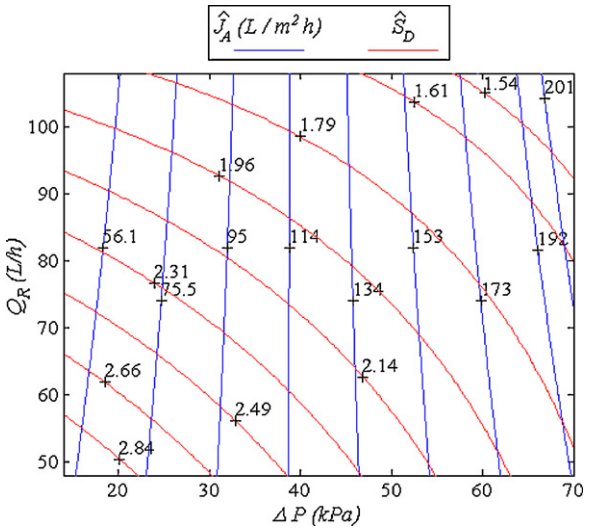

Fig. 14. Overlap contours plot of response surfaces for $W = 2800$ rpm.

The overlap contour map shown in Fig. 14 indicates that for the highest turbulent conditions (i.e. $W = 2800$ rpm), the average permeate flux J_A will grow and cumulative flux decline S_D will decrease with increasing of both transmembrane pressure and retentate flow rate. Thus, the overlap contour plot analysis gave the following optimal point of operating hydrodynamic conditions: $\Delta P = 70$ kPa, $W = 2800$ rpm and $Q_R = 108$ L/h. This point lies on the boundary of the region of experimentation. In fact, the established optimal point is a factorial point (+1 +1 +1) in our FFD matrix (Table 4), i.e. point number 1. Thus, the effect of the optimal hydrodynamics conditions ($\Delta P = 70$ kPa, $W = 2800$ rpm and $Q_R = 108$ L/h) upon the permeate flux behavior is given in Fig. 2a. As one can see from Fig. 2a the average permeate flux in the optimal conditions is the maximal one and the flux decline is the most reduced.

For the optimum hydrodynamic conditions of crossflow PAUF the rejection efficiency was determined using an optimal amount of polymer of $r = 5.88$. Likewise, the rejection of cobalt without adding polymer was assessed in order to figure out if there is some membrane–solute interaction. The results concerning the rejection efficiency for these both cases are shown in Fig. 15. As one can see, there is a significant difference between the rejections obtained with and without adding of polymer (PEI). In the presence of polymer, the cobalt rejection was about 90%. Surely, this value is lower than the rejection of 96.65% obtained for the same complexation conditions using the regenerated cellulose membrane and dead-end system (see part 1 of the work). This may be attributed to the fact that tubular metallic membrane used in crossflow experiments is less dense than flat sheet cellulose membrane. Concerning the rejection when no polymer is added, Fig. 15 shows clearly that there is no rejection without adding of polymer. In fact for this case the rejection is fluctuating near zero within the limits of experimental error of ±3%. Thus, the membrane–solute interaction is negligible.

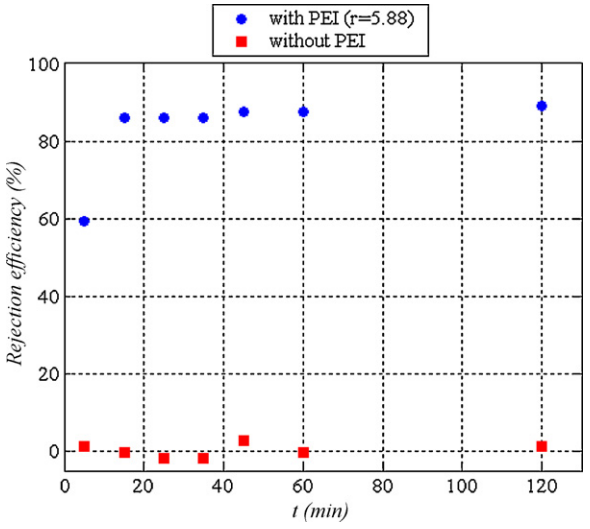

Fig. 15. Rejection efficiency determined for optimal conditions of crossflow PAUF: $[Co^{2+}]_0 = 65$ mg/L; pH 6.84; $P = 70$ kPa; $Q = 108$ L/h and $W = 2800$ rpm and for both cases (a) with adding of polymer (PEI) and (b) without polymer.

4. Conclusions

The crossflow ultrafiltration experiments dealing with cobalt removal from synthetic wastewaters by prior complexation with PEI were carried out in a homemade membrane module with rotating inner cylinder to promote turbulence and to reduce membrane fouling. The operating hydrodynamic conditions were planned according to full factorial experimental design and the kinetics curves of permeate flux decline were determined experimentally.

The experimental results revealed that the high rotation frequency led to improvement of permeate flux, normalized flux and membrane permeability. Also, the rotation may cause the self-cleaning effects resulting in the reduction of polymer layer thickness on the membrane surface due to turbulent hydrodynamic conditions.

The self-cleaning effect obtained for conditions of $\Delta P = 70$ kPa and $W = 1000$ rpm involves three distinguished stages within time. In the first moments, i.e. stage-I ($t < 30$ min), the permeate flux decline is the highest because of the transmembrane pressure effect. For stage-II ($30 \leq t \leq 120$ min), permeate flux begins to rise as a result of stronger effect of rotation frequency. The last stage-III ($t > 120$ min) is characterized by stabilizing of permeate flux as a result of achieving of equilibrium state between the effects of transmembrane pressure and rotation frequency.

The optimal hydrodynamic conditions in membrane module with rotating part was established by means of response surface methodology and overlap contour plot analysis for two selected responses, i.e. average permeate flux J_A and cumulative flux decline S_D. In the optimal hydrodynamic conditions of $\Delta P = 70$ kPa, $Q_R = 108$ L/h and $W = 2800$ rpm the maximal permeate flux and the minimal flux decline were observed.

Acknowledgements

The authors acknowledge the financial support of this research work from FP6 European Funds under Marie Curie project: AMERAC no. MTKD-CT-2004-509226.

References

[1] J.P. Kim, J.J. Kim, Flux enhancement with glass ball inserted membrane module for the ultrafiltration of dextran solution, Korean J. Chem. Eng. 20 (1) (2003) 99–103.
[2] L. Broussous, P. Schmitz, H. Boisson, E. Prouzet, A. Larbot, Hydrodynamic aspects of filtration antifouling by helically corrugated membranes, Chem. Eng. Sci. 55 (2000) 5049–5057.
[3] G. Zakrzewska-Trznadel, M. Harasimowicz, A. Miskiewicz, A. Jaworska, E. Dluska, S. Wronski, Reducing fouling and boundary-layer by application of helical flow in ultrafiltration module employed for radioactive wastes processing, Desalination 240 (1–3) (2009) 108–116.
[4] M.Y. Jaffrin, Dynamic shear-enhanced membrane filtration: a review of rotating disks, rotating membranes and vibrating systems, J. Membr. Sci. 324 (1-2) (2008) 7–25.
[5] D. Sarkar, C. Bhattacharjee, Modeling and analytical simulation of rotating disk ultrafiltration module, J. Membr. Sci. 320 (1–2) (2008) 344–355.
[6] M. Mellal, M.Y. Jaffrin, L.H. Ding, C. Delattre, P. Michaud, J. Courtois, Separation of oligoglucuronans of low degrees of polymerization by using a high shear rotating disk filtration module, Sep. Purif. Technol. 60 (1) (2008) 22–29.

[7] N. Moulai-Mostefa, O. Akoum, M. Nedjihoui, L. Ding, M.Y. Jaffrin, Comparison between rotating disk and vibratory membranes in the ultrafiltration of oil-in-water emulsions, Desalination 206 (1–3) (2007) 494–498.
[8] C. Bhattacharjee, P.K. Bhattacharyam, Ultrafiltration of black liquor using rotating disk membrane module, Sep. Purif. Technol. 49 (3) (2006) 281–290.
[9] S. Bhattacharjee, S. Datta, C. Bhattacharjee, Performance study during ultrafiltration of Kraft black liquor using rotating disk membrane module, J. Clean. Prod. 14 (5) (2006) 497–504.
[10] M.Y. Jaffrin, L.H. Ding, O. Akoum, A. Brou, A hydrodynamic comparison between rotating disk and vibratory dynamic filtration systems, J. Membr. Sci. 242 (1–2) (2004) 155–167.
[11] R. Bouzerar, P. Paullier, M.Y. Jaffrin, Concentration of mineral suspensions and industrial effluents using a rotating disk dynamic filtration module, Desalination 158 (1–3) (2003) 79–85.
[12] S.S. Lee, A. Burt, G. Russotti, B. Buckland, Microfiltration of recombinant yeast cells using a rotating disk dynamic filtration system, Biotechnol. Bioeng. 48 (4) (2004) 386–400.
[13] L.H. Ding, O. Akoum, A. Abraham, M.Y. Jaffrin, High shear skim milk ultrafiltration using rotating disk filtration systems, AIChE J. 49 (9) (2004)2433–2441.
[14] R. Bouzerar, M.Y. Jaffrin, L. Ding, P. Paullier, Influence of geometry and angular velocity on performance of a rotating disk filter, AIChE J. 46 (2) (2004)257–265.
[15] A. Brou, M.Y. Jaffrin, L.H. Ding, J. Courtois, Microfiltration and ultrafiltration of polysaccharides produced by fermentation using a rotating disk dynamic filtration system, Biotechnol. Bioeng. 82 (4) (2003) 429–437.
[16] U. Frenander, A.S. Jonson, Cell harvesting by cross-flow microfiltration using a shear-enhanced module, Biotechnol. Bioeng. 52 (3) (2000) 397–403.
[17] G. Naja, B. Volesky, A. Schnell, Comparative testing of tangential microfiltration for microbial cultures, Biotechnol. Bioeng. 95 (4) (2006) 584–598.
[18] C. Cojocaru, G. Zakrzewska-Trznadel, Response surface modeling and optimization of copper removal from aqua solutions using polymer assisted ultrafiltration, J. Membr. Sci. 298 (2007) 56–70.
[19] W. Shi, M.M. Benjamín, Membrane interactions with NOM and an adsorbent in a vibratory shear enhanced filtration process (VSEP) system, J. Membr. Sci. 312 (1-2) (2008) 23–33.
[20] A.I. Zouboulis, M.D. Petala, Performance of VSEP vibratory membrane filtration system during the treatment of landfill leachates, Desalination 222 (1–3) (2008) 165–175.
[21] R. Bian, K. Yamamoto, Y. Watanabe, The effect of shear rate on controlling the concentration polarization and membrane fouling, Desalination 131 (1–3) (2000) 225–236.
[22] K. Takata, K. Yamamoto, R. Bian, Y. Watanabe, Removal of humic substances with vibratory shear enhanced processing membrane filtration, Desalination 117 (1–3) (1998) 273–282.
[23] B.J. Bellhouse, G. Costigan, K. Abhinava, A. Merry, The performance of helical screw-thread inserts in tubular membranes, Sep. Purif. Technol. 22–23 (2001) 89–113.
[24] L. Broussous, E. Prouzet, L. Beque, A. Larbot, An experimental study of helically stamped ceramic microfiltration membranes using bentonite suspensions, Sep. Purif. Technol. 24 (2001) 205–221.
[25] T. Kluge, A. Kalra, G. Belfort, Viscosity effects on Dean vortex membrane microfiltration, AIChE J. 45 (9) (2004) 1913–1926.
[26] H. Mallubhotla, E. Nunes, G. Belfort, Microfiltration of yeast suspensions with self-cleaning spiral vortices: possibilities for a new membrane module design, Biotechnol. Bioeng. 48 (4) (1995) 375–385.
[27] G.A. Ameer, E.A. Grovender, B. Obradovic, C.L. Cooney, R. Langer, RTD analysis of a novel Taylor–Couette flow device for blood detoxification, AIChE J. 45 (3) (2004) 633–638.
[28] I. Siomina, S. Ahlinder, Lean optimization using supersaturated experimental design, Appl. Numer. Math. 58 (2008) 1–15.
[29] M.A. Bezerra, R.E. Santelli, E.P. Oliveira, L.S. Villar, L.A. Escaleira, Response surface methodology (RSM) as a tool for optimization in analytical chemistry, Talanta 76 (5) (2008) 965–977.
[30] T. Lundstedt, E. Seifert, L. Abramo, B. Thelin, A. Nystrom, J. Pettersen, R. Bergman, Experimental design and optimization, Chemometr. Intell. Lab. 42 (1998) 3–40.
[31] D. Vishal, K.V. Karate, Marathe, Simultaneous removal of nickel and cobalt from aqueous stream by crossflow micellar enhanced ultrafiltration, J. Hazard. Mater. 157 (2–3) (2008) 464–471.
[32] J.S. Yanga, K. Baekb, J.W. Yang, Crossflow ultrafiltration of surfactant solutions, Desalination 184 (2005) 385–394.
[33] K. Vasanth Kumar, K. Porkodi, F. Rocha, Comparison of various error functions in predicting the optimum isotherm by linear and non-linear regression analysis for the sorption of basic red 9 by activated carbon, J. Hazard. Mater. 150 (2008) 158–165.